Spatial and Temporal Variability of Water-Filled Crevasse Hydrologic States Along the Shear Margins of Jakobshavn Isbrae, Greenland

Casey A. Joseph

A scholarly paper in partial fulfillment of the requirements for the degree of

Master of Science

May, 2018

Department of Atmospheric and Oceanic Science, University of Maryland
College Park, Maryland

Advisor: Dr. Derrick Lampkin

Table of Contents

Abstract

The impact of melt water injection into ice streams over the Greenland Ice Sheet is not well understood. Water-filled crevasses along the shear margins of Jakobshavn Isbræ are known to fill and drain, resulting in weakening of the shear margins due to reduced basal friction. Additionally, seasonal variability in the hydrologic dynamics of these features has not been quantified. In this work, we characterize the spatial and temporal variability in the hydrological state (filled or drained) of 7 groups of crevasse (CV) systems. A fusion of multi-sensor optical satellite imagery was used to examine hydrologic states during the melt season (May to September) from 2000 to 2015. The peak number of days in the monthly distribution of filled crevasse systems was during the month of July at 329 days, while May had the least at 15. Over the study period the occurrence of drainage within a given season increased. The number of drainages per crevasse group in a season ranged from 0 to 5. The frequency of multi-drainage events were correlated with large strain rates. Over the study period, average summer temperatures ranged from -1 and 2 ⁰C, and tensile strain rates have increased to as high as ~ 1.2 a^{-1} . Drainage due to fracture propagation may be increasingly modulated by ocean-induced calving for lower elevation systems. Overall water-filled crevasses could expand in extent and volume as temperatures increase resulting in regional amplification of ice mass flux through Jakobshavn Isbræ.

Acknowledgements

List of Tables

List of Figures

List of Symbols

Ψ Water-filled crevasse hydrologic state

$\dot{\varepsilon}$ Horizontal Strain Rate

y_i Logit regression response variable

$\boldsymbol{\beta}$ Vector of regression coefficients

t_n Time for only days a direct observation was recorded

$\widehat{var}\beta_j$ Standard error of the logit model

N_{fill} Cumulative days over which a crevasse group was filled

ζ Number of drainages

$<T>$ Average summer temperature

$\bar{D}_{CV1}$ Distance between crevasse group 1 and the terminus of Jakobshavn Isbrae

ΔD_f Inter-seasonal changes in front location

ΔD_{CV} Magnitude of observed frontal change

Chapter 1 Introduction

1.1 Motivation and Prior Work

The Greenland Ice Sheet (GrIS) has experienced considerable mass loss over the last few decades (Alley, Clark, et al., 2005; Alley, Dupont, et al., 2005; Hanna et al. 2008; Joughin et al. 2004; Krabill et al. 2004; Luthcke et al. 2006) resulting in negative mass balance and substantive contribution to sea level rise (Rignot et al. 2008; Shepherd et al. 2012; van den Broeke et al. 2009). Commensurate with these changes has been the documented impact of surface meltwater on ice sheet velocity during the summer within the ablation zone (Bartholomew et al. 2010; Hoffman et al. 2011; Joughin et al. 2008; Palmer et al. 2011; Shepherd et al. 2009; Sundal et al. 2011; van de Wal et al. 2008; Zwally et al. 2002), via supraglacial lakes, channels, and moulins largely beyond regions of fast flow (Box & Ski, 2007; Das et al. 2008; Echelmeyer et al. 1991; Howat et al. 2013; Joughin et al. 1996; Koenig et al. 2015; Lampkin 2011; McMillan et al. 2007; Selmes et al. 2011; Sneed & Hamilton 2007; Sundal et al. 2009; Tedesco & Steiner 2011). However, the presence of ponded water within regions of fast flow has received little attention. Lampkin et al. (2013) evaluated the spatial and temporal variability of water-filled crevasse filling and drainage dynamics during the 2007 melt season within the shear margins of Jakobshavn Isbræ. Crevasses at elevations less than ~500 m start to fill around June 6 with a total area of ~0.15 km^2. A peak total area of ~1.8 km^2 was reached in early July with most groups still maintaining some water on August 9, 2007. Water-filled crevasse systems filled and drained at rates as large as 0.03 km^2 d^{-1} and 0.012 km^2 d^{-1} respectively (Lampkin et al. 2013). These systems likely drain resulting from the vertical propagation of fractures to the bedrock via hydrofracture (Alley,

8

Dupont, et al. 2005; Benn et al. 2007; Das et al. 2008; Krawczynski et al. 2009; Nye 1955, 1957; Van der Veen 1998, 1999). A fracture will propagate to a depth where the stress intensity factor is equal to the fracture toughness, and can even reach the bedrock if a region is under tension (Van der Veen 1998, 2007). Lampkin et al. (2013) establish that local strain rates are sufficient to drive fractures through to the bed for most crevasse (CV) groups. These features have the capacity to inject substantial volumes of water into the shear margins equivalent to the largest supraglacial lakes found outside of the ice stream (Lampkin et al. 2013). However, we do not understand how these crevasse systems have changed over time, their specific impact on regional ice dynamics, and the mechanisms through which melt water from these features can be delivered to the bedrock.

1.2 Objective

This investigation performs the most comprehensive assessment of the spatial and temporal variability of water-filled crevasses along the shear margins of Jakobshavn Isbrae (Figure 1).
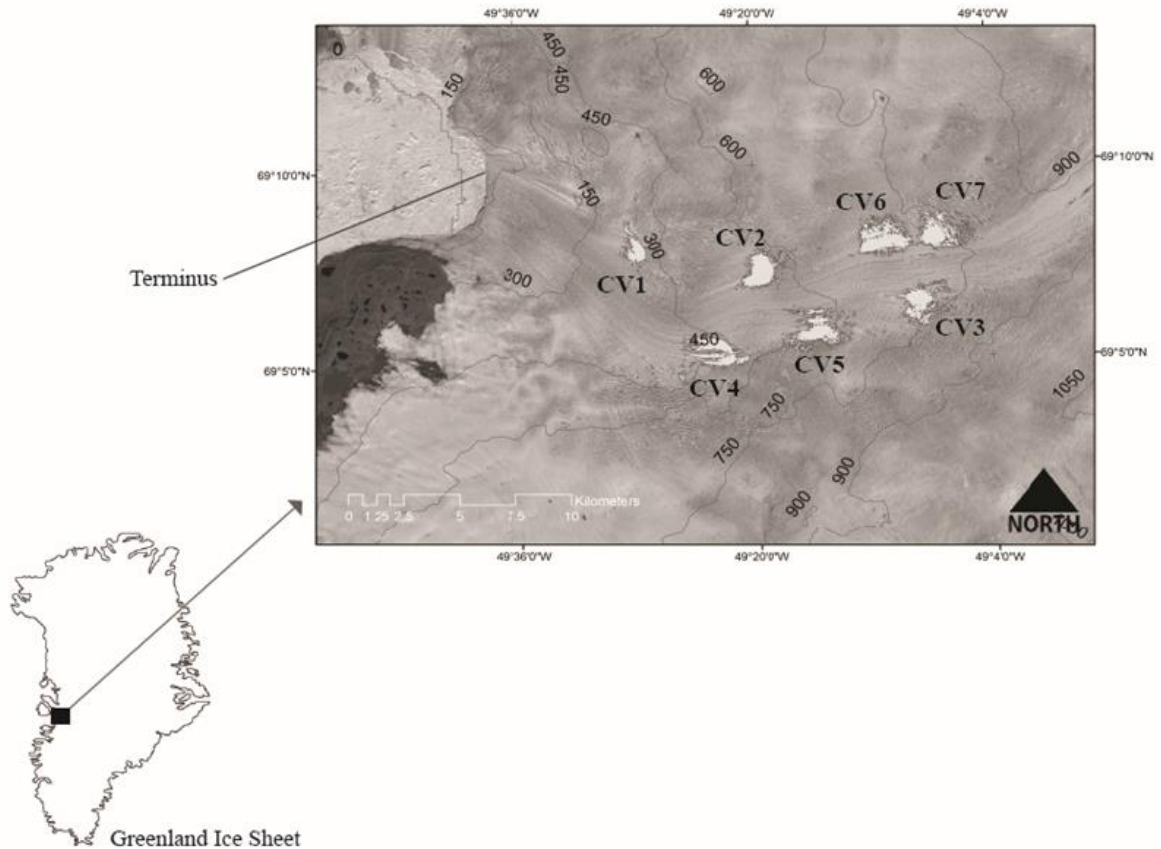
Figure 1. Study area showing the location of water-filled crevasse systems (CV) (white) within the shear margins of Jakobshavn Isbræ, west-central Greenland. The spatial extent is a composite based on observed areal extent from cloud-free, Landsat-7 panchromatic imagery only from 2000-2013. Contours of elevation in meters are superimposed.

We seek to characterize variability in drainage dynamics over water-filled crevasse systems at annual and interannual time scales using a fusion of multi-sensor data from several optical satellite systems acquired over a 16 year period from 2000 to 2015 each season during the period from May to September. We restrict our assessment to characterizing the 'hydrologic state' (filled or drained) of these 7 water-filled crevasse systems over the analysis period. We do not quantify changes in the volume or areal extent of these systems. We characterize temporal patterns in the drain state of water-filled crevasse systems responsible for hydrologic weakening of Jakobshavn Isbrae

(Lampkin et al. 2013). We also explore first-order controls on observed drainage behavior. This work provides an important benchmark from which future changes in this component of supraglacial hydrology and the role of meltwater in fast flowing ice streams will be evaluated. The results from this study have implications for understanding processes driving mass discharge from marine-terminating outlet glaciers throughout GrIS.

Chapter 2. Data

2.1 Satellite Imagery

Satellite imagery was acquired from several optical satellite systems spanning a range in performance capacity. Cloud-free images from seven imaging systems were used to quantify the hydrologic state of each water-filled crevasse system. The presence of ponded water is easily identified in imagery acquired over the visible part of the electromagnetic spectrum resulting from the propensity for water to absorb incoming solar radiation more effectively than the surrounding ice and firn (Lampkin & VanderBerg 2011). Data from Landsat-7 ETM+, Landsat-8 OLI, Quickbird-1/2, Geo-Eye, Worldview-1/2, EO-1 ALI, SPOT-5 and ASTER, were used in this analysis. The combination of data from these systems increases the frequency of sampling resulting in enhanced temporal resolution which offsets the impact of cloud cover. The number of cloud-free images varies for each satellite system, resulting in a non-periodic sampling interval. The overall temporal resolution was improved, though the sampling rate was inconsistent. For more details on imagery and data sources see Table 1.

Imaging System	Spatial Resolution (m)	Temporal Resolution (days)	Source
Landsat-7 ETM+	30 (multispectral)/15 (pan)	16	United States Geological Survey
Landsat-8 OLI	30 (multispectral)/15 (pan)	16	United States Geological Survey
Quickbird-2 Worldview-1/2 GeoEye-1	1.84 (multispectral)/0.46 (pan) 0.5 1.84 (multispectral)/0.46 (pan)	11 1.7 8.3 (max)	Polar Geospatial Center
EO-1 ALI	30 (multispectral)/10 (pan)	16	United States Geological Survey
SPOT-5	10 (multispectral)/5 (pan)	2-3	Airbus Defense & Space
ASTER	15 visible/NIR	16	United States Geopolitical Survey
Google Earth†	------	---	Google Earth

†Google earth Images are derived from several satellite systems including Quickbird, Worldview, and Geo-Eye.

Table 1: Summary of Satellite Data

2.2 Surface Temperature Data

Near surface temperature data were acquired from the Greenland Climate Network (GC-

Net) near Jakobshavn Isbrae from the Cooperative Institute for Research in

Environmental Sciences (CIRES) (Steffen et. al. 1996). Hourly 2 m surface temperatures sampled at the JAR 1 and Swiss Camp GC-NET stations were used to create a composite daily average temperature. This time series was used to evaluate patterns in the filling and drainage variability of water-filled crevasse systems.

2.3 Velocity Data

Velocity data used in this analysis were derived from the National Science and Ice Data Center (NSIDC) MEaSUREs data archive on Greenland Ice Velocity: Select Glaciers InSAR (release v1.1) (Joughin et al. 2016) (http://nsidc.org/data/nsidc-0481/). Surface velocity fields were derived from TerraSAR-X (TSX) image pairs based on speckle tracking and interferometric techniques (Joughin et al. 2010, 2016). Available transverse and longitudinal component surface velocity grids were acquired from this archive over the Jakobshavn Isbrae study area from 2009 to 2015 during the months of May through August. Nominal spatial resolution of these grids are at 100 m.

2.4 Elevation Data

Elevation data used in this analysis were derived from the NSIDC MEaSUREs Greenland Ice Mapping Project (GIMP) Digital Elevation Model (Howat et al. 2015a, 2015b) (http://nsidc.org/data/docs/measures/nsidc-0645/). This DEM was created using a combination of ASTER and SPOT 5 DEMs over the ice sheet periphery and margin south of 82.5° N, and Advanced Very High Resolution Radiometer (AVHRR) photoclinometry for the ice sheet interior and far north. Land elevations were calibrated to 2003-2009

average ICESat and Geoscience Laser Altimeter System (GLAS) elevations (Howat et al. 2015a).

2.5 Calving Front Location

Calving front location (terminus) information were acquired from the European Space Agency (ESA) Climate Change Initiative (CCI) Greenland Ice Sheet Essential Climate Variables data archive (http://esa-icesheets-greenland-cci.org/) (Nagler et al. 2017). Calving front positions were delineated manually through visual interpretation and digitization of satellite imagery annually. ERS and ENVISAT Synthetic Aperture Radar (SAR) imagery, and optical data from Landsat 5, 7, and 8 platforms were used to build the terminus location archive. Terminus positions were assessed for 22 of GrIS 28 major marine-terminating outlet glaciers. We acquired calving front location data over Jakobshavn Isbræ from 2002 to 2015.

Chapter 3. Methods

3.1 Determination of Hydrologic State of Water-filled Crevasses

The hydrologic state of water-filled crevasse systems (ψ) were quantified through visual interpretation of imagery. The occurrence or presence of water within the water-filled crevasse groups indicate a filled ($\psi=1$) hydrologic state, while the absence defines a drained ($\psi=0$) state. A crevasse group was assumed to remain filled until a subsequent image indicates that a particular group is devoid of water. We assumed a given crevasse group remained water-filled during intervening periods when conditions prevented direct

observation. This scenario can occur when an initial cloud-free image displays water in a system and is followed by a period of cloud-covered or lack of available images. After such a period, if the subsequent image no longer showed water present then we assumed drainage occurred during the intervening interval. In general, when a crevasse was observed to be filled, we assumed the crevasse was filled until we either observed the crevasse to drain, or the study period for that given year ended. We did not document the areal extent of ponds and did not record partial drainage events. If water was present at all regardless of pond size, we designate the pond as "filled" otherwise it is classified as "drained".

3.2 Derivation of Strain Rate

The surface velocity field was decomposed into components consisting of vector (u) oriented in the prevailing direction of ice flow (x) within the main trough of the ice stream, and an orthogonal component (v) perpendicular to ice flow (y). Horizontal strain rates ($\dot{\varepsilon}$) were estimated from measured surface velocity through differentiation of component velocity grids where the strain rate tensor is given by:

$$\begin{bmatrix} \dot{\varepsilon}_x & \dot{\varepsilon}_{xy} \\ \dot{\varepsilon}_{yx} & \dot{\varepsilon}_y \end{bmatrix} = \begin{bmatrix} \frac{\partial u}{\partial x} & \frac{1}{2}\left(\frac{\partial u}{\partial y} + \frac{\partial v}{\partial x}\right) \\ \frac{1}{2}\left(\frac{\partial v}{\partial x} + \frac{\partial u}{\partial y}\right) & \frac{\partial v}{\partial y} \end{bmatrix} \qquad (1)$$

Strain rate component fields were used to calculate the magnitude in the principle strain axis in the horizontal plane, where the magnitude of minimum ($\dot{\varepsilon}_1$) and maximum ($\dot{\varepsilon}_3$) tensile strains are given by:

$$\dot{\varepsilon}_1 = \frac{1}{2}\left(\dot{\varepsilon}_x + \dot{\varepsilon}_y\right) - \sqrt{\left[\frac{1}{4}\left(\dot{\varepsilon}_x - \dot{\varepsilon}_y\right)^2 + \dot{\varepsilon}_{xy}^2\right]} \qquad (2)$$

$$\dot{\varepsilon}_3 = \frac{1}{2}(\dot{\varepsilon}_x + \dot{\varepsilon}_y) + \sqrt{\left[\frac{1}{4}(\dot{\varepsilon}_x - \dot{\varepsilon}_y)^2 + \dot{\varepsilon}_{xy}^2\right]} \qquad (3)$$

In this analysis, we were specifically interested in the $\dot{\varepsilon}_3$ field as we wanted to examine the spatial and temporal variability in the tensile strain field, which controls fracture propagation within the shear margins. Given this, we did not compute the angle between $\dot{\varepsilon}_1$ and $\dot{\varepsilon}_3$. All grids based on velocity image pairs of estimated $\dot{\varepsilon}_3$ between May and August of each season were averaged. The seasonal averages values were sampled within the maximum areal extent of water-filled crevasse system delineated from Landsat ETM imagery during the 2007 melt season (Lampkin et al., 2013) and spatially averaged $\overline{(\dot{\varepsilon}_3)}$.

3.3 Logistic Regression Modeling

We implemented a logistic (logit) regression model to assess temporal changes in the hydrologic state of water-filled crevasses over the analysis period. The use of logit regression was appropriate as our response variable (y_i) was binary (0 or 1) where

$$y_i = \begin{cases} 1 & \text{if crevasse was water filled} \\ 0 & \text{if crevasse was completly empty} \end{cases} \qquad (4)$$

Here y_i is considered the realization of a random variable Y_i that can take binary values with probabilities π_i and $1 - \pi_i$ respectively. The distribution of Y_i is a binomial distribution in which probabilities are expressed as

$$Pr\{Y_i = y_i\} = \pi_i^{y_i}(1 - \pi_i)^{1-y_i} \qquad (5)$$

assuming observations on y_i were independent. Given this we defined a model such that π_i is a linear function of covariates

$$\pi_i = x'\beta \qquad (6)$$

where $\boldsymbol{\beta}$ is a vector of regression coefficients. This ordinary least squares model was transformed to accommodate a binary dependent variable through the logit transform through expressing probabilities as odds ($\frac{\pi_i}{1-\pi_i}$) and deriving the log-odds given by

$$logit(\pi_i) = x'\boldsymbol{\beta} \tag{7}$$

where the fitted model in Eq. (7) using the maximum likelihood estimation routine computes $\boldsymbol{\beta}$, which represents the change in the logit of the probability associated with a unit change in the independent variable assuming all else held constant. Solving for the probabilities resulted in the transformed model as

$$\pi_i = \frac{e^{\{x'\beta\}}}{1+e^{\{x'\beta\}}} \tag{8}$$

Our model is built such that the dependent variable was the observed hydrologic state, and the independent variable is time (t_n) for only days a direct observation was recorded (non-interpolated). In this analysis, we were primarily interested in the change in the probability of filled states over time. This was accomplished through hypothesis testing on the modeled $\boldsymbol{\beta}$ coefficient. We employed the Wald statistical test, which tests the significance of the null hypothesis ($\boldsymbol{H}_0$: $\beta_j = 0$) at the 5% significance level, by calculating a metric (z) with a χ^2 distribution when $\boldsymbol{H}_0$ is true given by

$$\hat{z} = \left(\frac{\beta_j}{\sqrt{\widehat{var}(\beta_j)}}\right)^2 \tag{9}$$

where $\widehat{var}\beta_j$ is the standard error (deviation) of the model.

Chapter 4. Results

4.1 Spatial and Temporal Variability of Hydrologic State

The availability of cloud-free images varied across the study period with some years having more samples than others. The number of total samples per season increased with time (Figure 2a).
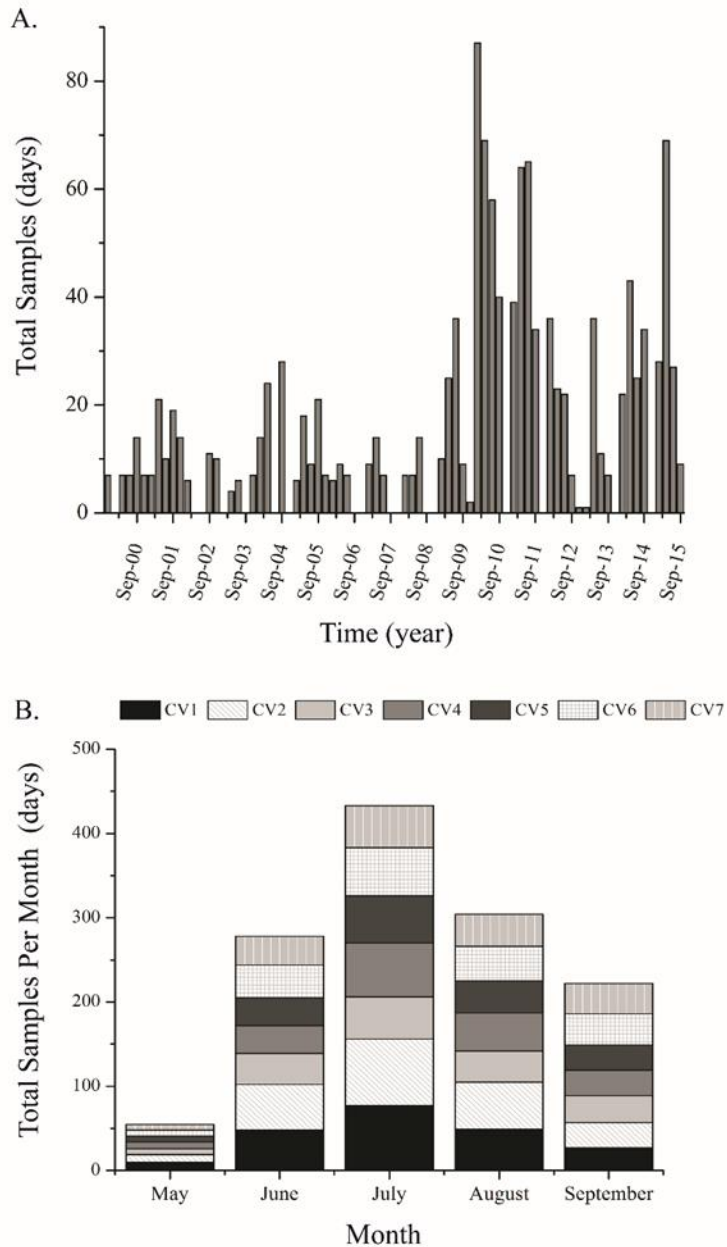
Figure 2. (a) Time series of total monthly cloud-free, optical images from various sensors (Table 1) over the study period from 2000 to 2015. **(b)** Cumulative number of cloud-free optical images over the 16 year study period for each water-filled crevasse group per month during the ablation season (May to September).

The maximum scenes available for any given month in the study period was 87 in June 2010. There were 17 months in the study period that cloud-free imagery was not available (Figure 2a). The total number of images across all seven CV groups ranged from 163 to 228 scenes. The total number of cloud-free images varied for each crevasse system throughout the study period. The month of May maintained the least number of clear scenes at 55, while July had the most at 433 scenes (Figure 2b). The monthly distribution of filled crevasses over the 16 year study period was unimodal with a peak in the number of filled days during the month of July at 329 days, while May had the least at 15 days (Figure 3).
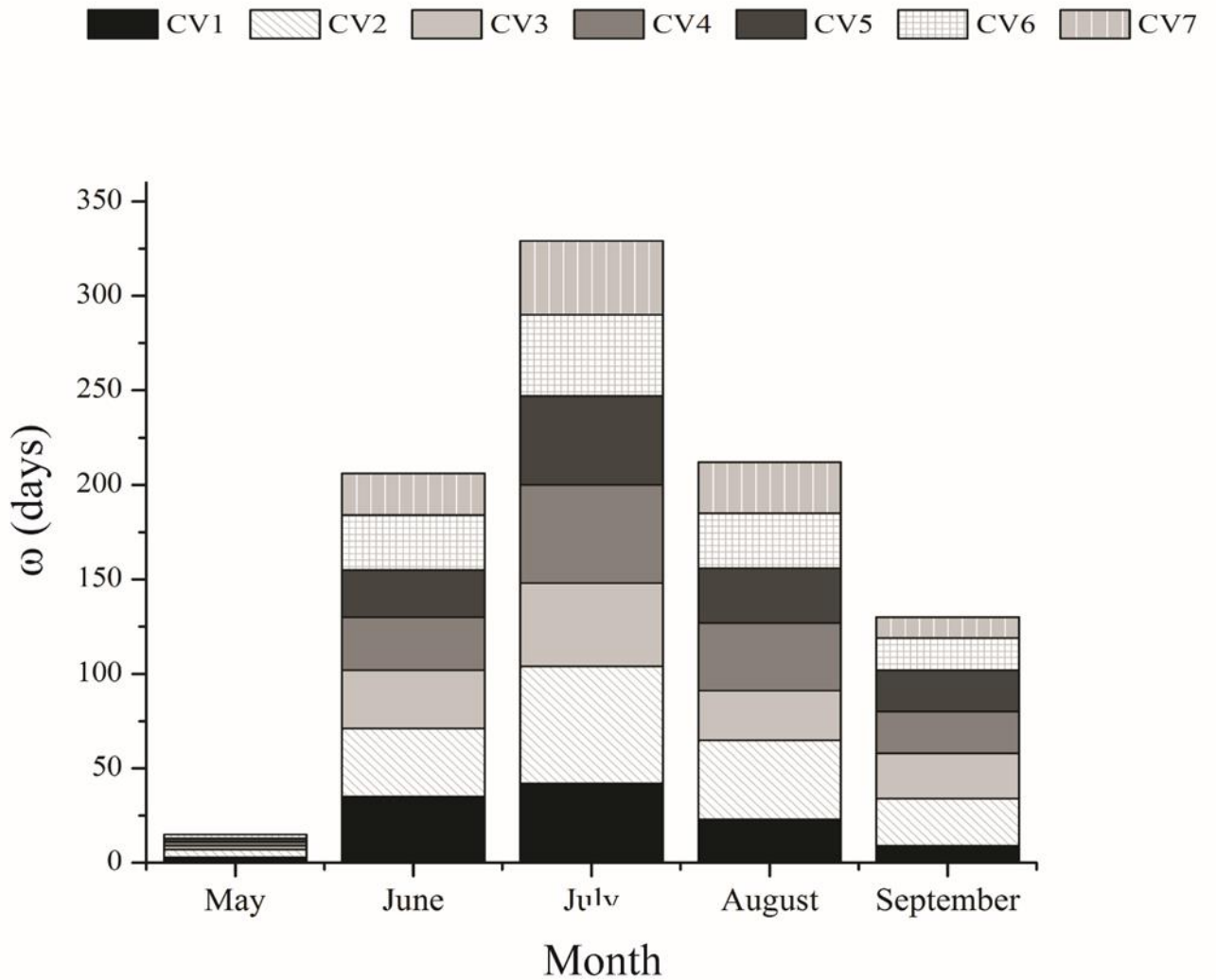
Figure 3. Cumulative monthly distribution of the total number of days over the 16 year study period where each water-filled crevasse system was observed from optical imagery to occupy the 'filled' hydrologic state.

Specifically, CV2 had the largest number of observed filled days among all the systems with 169 days, and CV7 had the least at 96 days. Days between observations were largely 10 days or less (Figure 4).
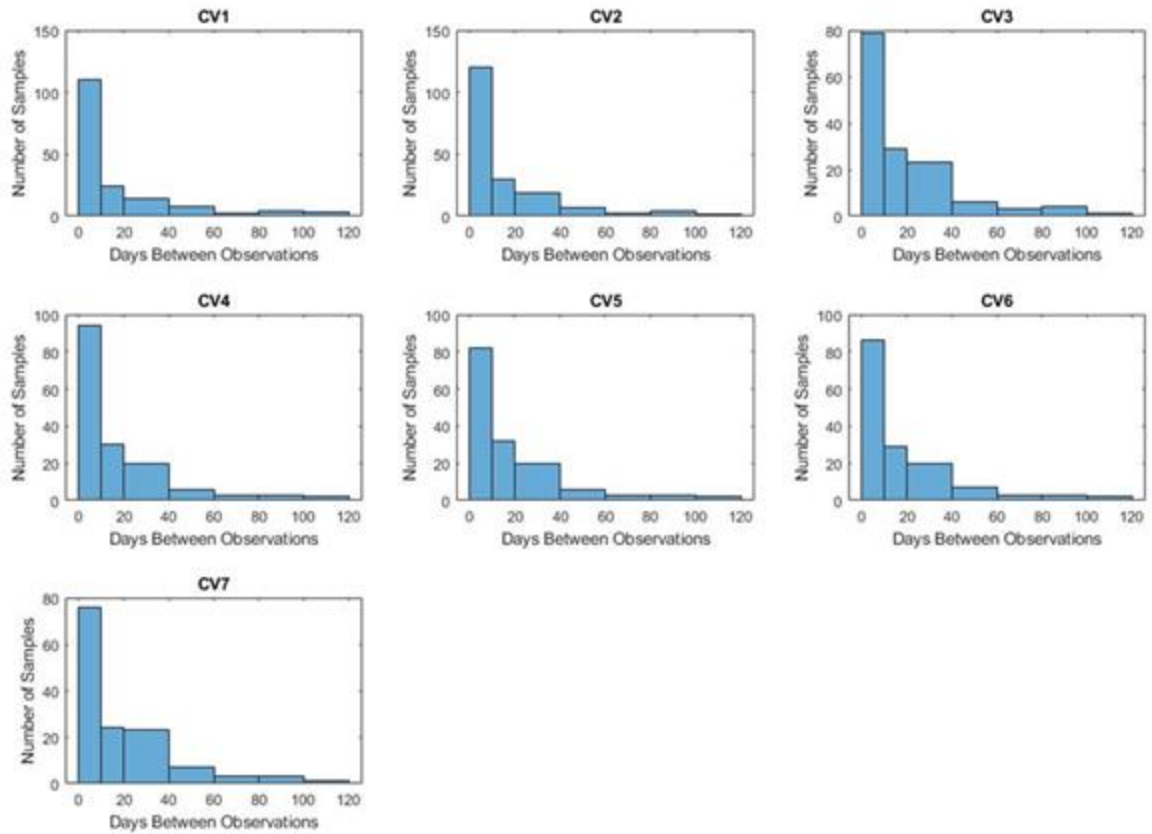
Figure 4: Histogram showing the days between subsequent observations for each CV group.

All CV groups had a minimum of 1 day between observations. The maximum days between observations was 140 for CV7, while the maximum days between observations was 107 for CV2 and 3. The maximum days between observations for CV4, 5, and 6 was 108 days, and 111 days for CV1. Total percent of days filled (interpolated) over the study period ranged from roughly 36-55% (Figure 5).
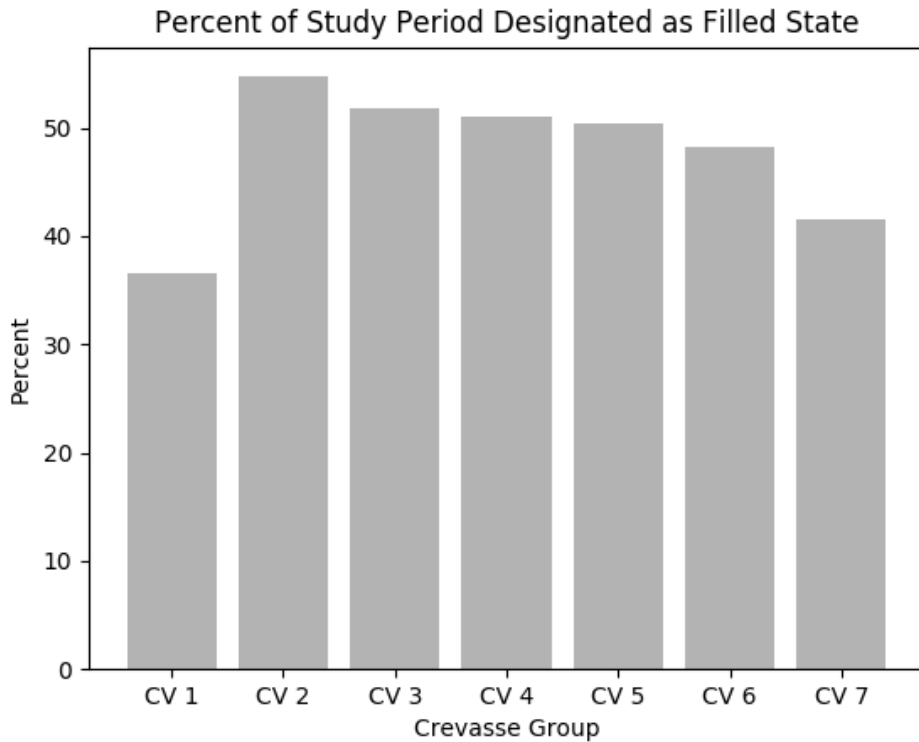
Figure 5: Cumulative percentage of days that each crevasse group was designated the filled state (interpolated) for the entire study period.

CV2 was filled for the longest duration, while CV1 was filled for the shortest duration over the entire study period.

4.2 Drain Frequency

Throughout the study period water-filled crevasse systems were observed to fill and drain throughout each season (Figure 3). Some systems were observed to refill and drain multiple times during a season, this will be referred to as a multi-drain event for the remainder of the paper. Over the 16 year study period, there were 9 seasons where at least one crevasse group demonstrated a multi-drain event. For the 2011 season 13 drainage events were observed, with CV1 draining 5 times, both of which were maximums for the

study. In 2003 we only observed 5 drainage events, indicating that 2 crevasse groups did not have water observed. Temporal patterns in seasonal hydrologic state over all crevasse groups was also examined. A time series of cumulative days over which crevasse systems were filled with water (N_{fill}) demonstrated five distinctive multi-year patterns (Figure 6a).
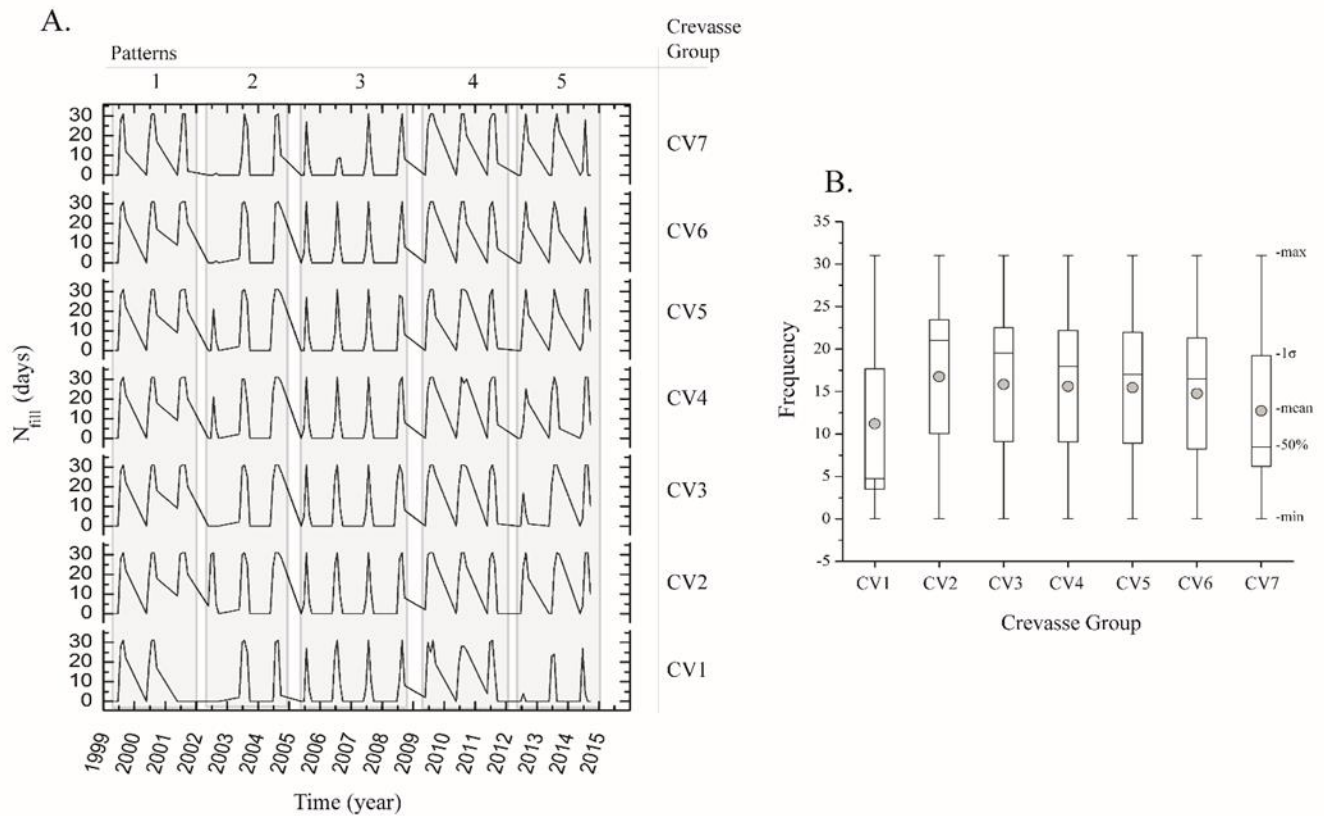
Figure 6. (a) Time series of cumulative monthly days that each crevasse group was filled over the study period. (b) Histogram showing the distribution in duration of filled hydrologic state (days) over the entire study period for each crevasse system. Plot shows mean (⊙), minimum and maximum (whiskers), 1σ (box edge), and 50% (line).

These patterns generally ranged between 3-4 years and were consistent across all groups. The mean number of filled days per month were evaluated (Figure 6b), and varied across the seven crevasse groups. All seven crevasse groups maintain the same range of filled days per month over the study period. CV1 had the lowest mean at 11.21 days, while CV2 had the maximum mean at 16.75 filled days per month. Mean filled days across all

groups were within 1σ of each other indicating that most groups did not demonstrate significant differences in the duration of filled states.

4.3 Relationships between Drain Frequency and Near-Surface Temperature

Relationships between drain frequency and near-surface atmospheric temperature were explored (Figure 7).
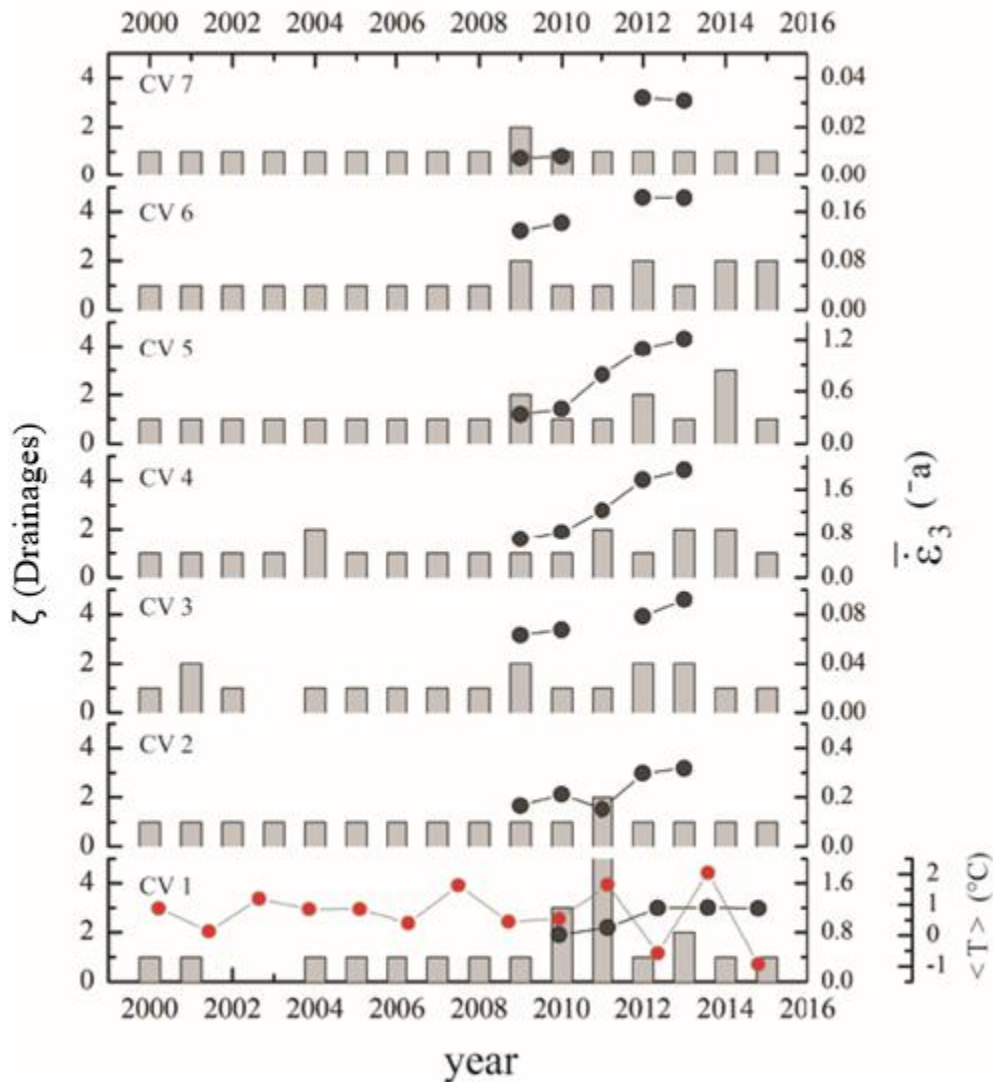
Figure 7. Time series of number of drainage events per year per crevasse group (ζ, gray bars) with average temperature (<T>) (●) derived from Greenland Climate Network (GC-Net) 2 m surface temperatures (°C) sampled at the JAR 1 and Swiss Camp stations superimposed on the lower panel. Mean maximum tensile strain rate (●) for each CV group estimated from measured surface velocity.

24

Average summer temperature ranged from -1 and 2 °C for each season. From 2000 to 2006, average summer temperatures varied only between 1 to 0 °C. Commensurately, water-filled crevasse groups only demonstrated single drainage events. After 2006 temperatures increased to as high as 2 °C and varied over a larger range as high as ~3 °C difference between successive seasons. During this period, the number of drainage events per season across all CV groups (except CV7) increased with some variation in year to year drainage count.

4.4 Relationships between Strain Rate and Drainage

Variations in $\bar{\dot{\varepsilon}}_3$ can be indicative of conditions that drive fracture propagation responsible for drainage of water-filled crevasses. Unfortunately, we were not able to correlate changes in strain rate with observed drain occurrence because we did not always have velocity data available for each crevasse group over every season. However, we were still able to identify some relationships between strain rate, and drainage. There were only 2 multi-drain events across all crevasse groups before 2009 (Figure 7). From 2009-2015 there were 20 multi-drain events across all crevasse groups. Generally, strain rates increased over most groups from 2009 to 2015. CV4, and 5 showed the largest increase in strain during this period of ~ 1.2 a^{-1} and 0.9 a^{-1} respectively. The range in tensile strain rate magnitudes varied across the water-filled crevasse groups. CV1, 4, and 5 demonstrated the largest magnitudes, while CV3, 6, and 7 were the lowest. Specifically, the CV1 group experienced an increase in multi-drain events in 2010 and 2011 with a commensurate increase in tensile strain, which reached a peak of ~1.2 a^{-1} with no further

changes afterwards. Interestingly, CV2 had only one season where it demonstrated multiple drainage events (2011). From 2009 to 2015, strain rates over CV2 increased slightly from 2009 to 2010 but decreased by 0.1 a^{-1} in 2011. After 2011, strain rates rose dramatically but CV2 returned to draining only once per season. The CV3 group experienced four multiple drainage events throughout the study period. Strain rates for CV3 were only available from 2009 to 2010 and 2012 to 2013. Strain rate values ranged from ~ 0.06 to 0.1 a^{-1}. Over these four seasons, CV3 maintained three multiple drainage events with 2010 being the exception. CV4 showed four seasons where multiple drainage events occurred. Strain data for this group was available from 2009-2013, showing increasing strain from ~0.8 to 2 a^{-1}. During this period, CV4 showed an increase in the occurrence of multiple drainage events. CV5 was similar and experienced an increase in multiple drainage events as well. CV6 was observed to experience four multi-drain years. CV6 and 7 had limited data available from which to estimate tensile strain rates. Therefore only the 2009, 2010, 2012, and 2013 seasons are shown. Strain rates over CV6 ranged from ~0.12 to 0.18 a^{-1}, which occurred during a period with a higher frequency in occurrence of multiple drainage events than the period before 2009. Lastly, CV7 had only one multiple drainage event throughout the entire study period during the 2009 season, which did not correlate to the observed periods of strain increases.

4.5 Relationship between Terminus Location and Drain Occurrence

Fluctuations in local strain rates in the vicinity of each CV group could be induced by downstream calving events at the glacier terminus. We tracked seasonal and inter-seasonal changes in calving front location from 2002 to 2015 (Figure 8).
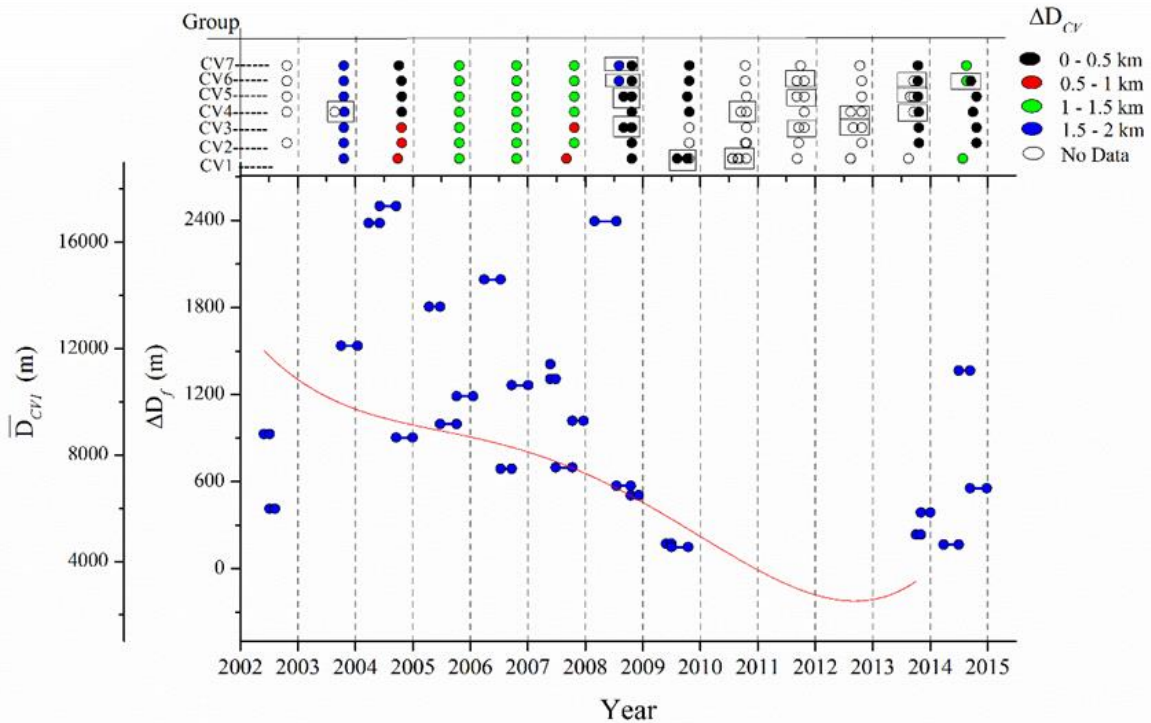
Figure 8. Relationships between the temporal evolution of Jakobshavn Isbræ terminal retreat and drain occurrence over each water-filled crevasse group from 2002 to 2015. Lower panel depicts seasonal change in distance between the lowest elevation crevasse system (CV1) and the terminus (red line) ($\bar{D}_{CVI}$). Additionally, the lower panel displays the inter-seasonal changes in front location (ΔD_f) where the (●) connected by a bar indicate the effective period over which the terminus retreated based on satellite observations. The top panel shows the magnitude of observed frontal change (ΔD_{CV}) displayed in 0.5 km categories, which corresponds to observed drainage events from our multi-sensor archive for each crevasse group.

Over this period of time, the terminus of Jakobshavn Isbræ had retreated inland substantially (Figure 8). We tracked the mean seasonal distance from the lowest elevation water-filled crevasses system (CV1) ($\bar{D}_{CVI}$) to the terminus. From 2002 to 2013 the terminus had retreated ~ 8 km towards CV1. By 2015, the glacier front was ~ 2 km away from CV1. Inter-seasonal changes in front location (ΔD_f) showed large variations over the analysis period. The shorter the interval over which the front locations were observed, the smaller the magnitude in front movement. The 2004 and 2008 summers showed the

largest magnitude in front retreat of ~ 2.5 km. Generally, the magnitude of change in frontal movement decreased over the analysis period.

Additionally, we examined relationships between front changes and the timing of drainage from each CV group over the study period (Figure 8, top panel). We documented the magnitude of observed frontal change (ΔD_{CV}) that corresponded to the time period when drainage was observed to occur from the water-filled crevasse groups. During the 2003 season, all CV groups drained during a period when $1.5 < \Delta D_{CV} < 2$ km. In 2004, CV1, 2, and 3 drainage events corresponded to $0.5 < \Delta D_{CV} < 1$ km, while the others corresponded to $0 < \Delta D_{CV} < 0.5$ km. The 2005, 2006, and 2007 seasons mainly demonstrated that ΔD_{CV} values ranged between 1 and 1.5 km for most CV groups. From 2009 to 2015, most drain occurrences tended to correspond to the smallest range in ΔD_{CV} (0 to 0.5 km) commensurate with an increase in multiple drainage events (boxes) (Figure 8, top panel).

4.6 Logit Model

A logistic regression analysis was conducted to evaluate the temporal variability in hydrologic state of water-filled crevasses. The time series for each CV system was fit with a logit model. The models provide an estimate of the probability of the crevasse group to be water-filled, $P(\psi=1)$. We were strictly concerned with evaluating the trend in the occurrence of ψ and not interested in using models to predict or interpolate hydrologic states. Generally, CV1, 5, and 6 maintained a decrease in $P(\psi=1)$ with time, while CV3 and 7 increased and CV4 was invariant (Figure 9).
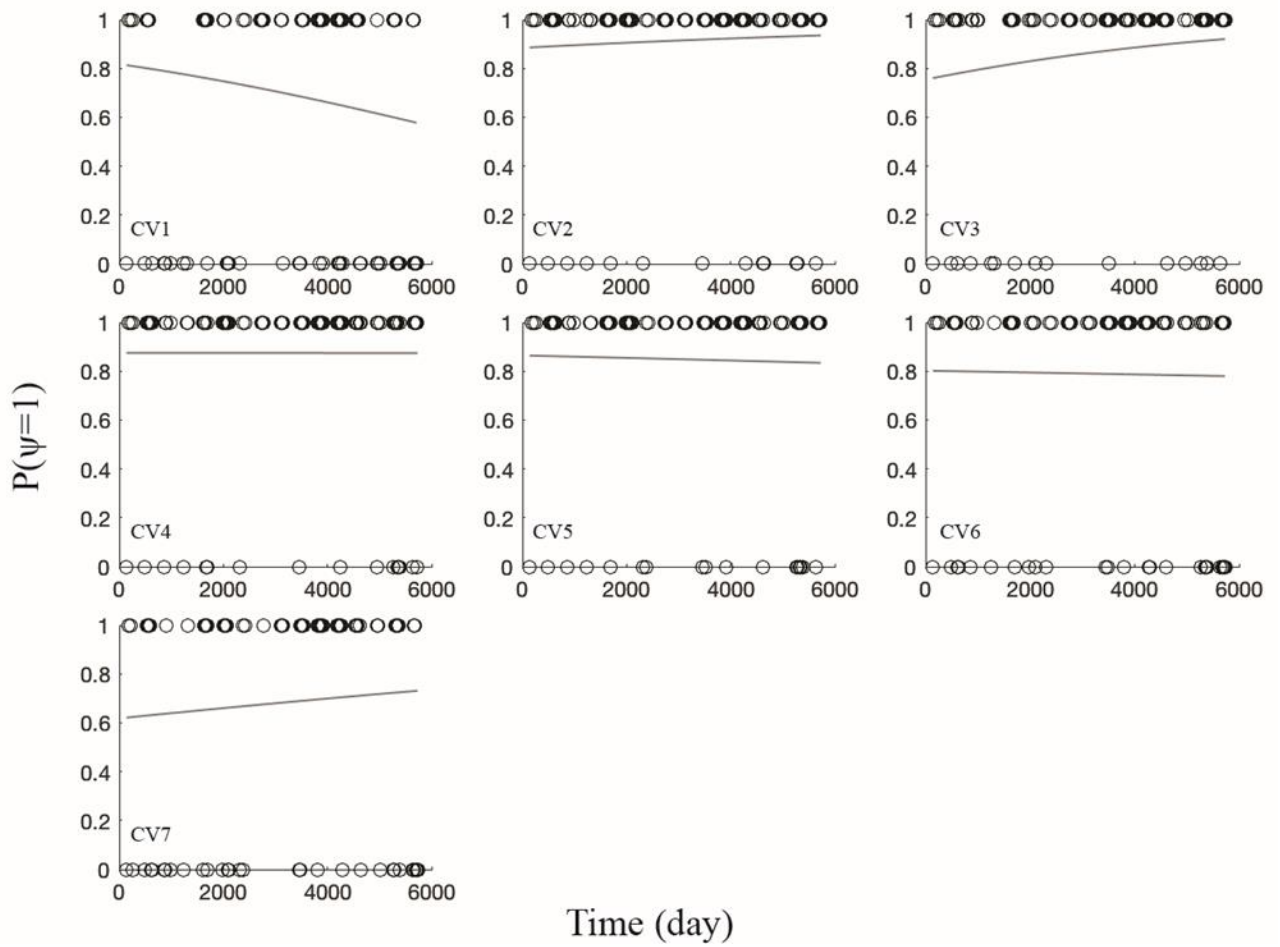
Figure 9. Logit regression analysis on the probability of filed state P(ψ=1) vs time for all crevasse groups over the study period. Circles are hydrologic states such that ψ=1 is filled and ψ=0 is drained. Solid line is logit model fit.

Significance test on the $\hat{z}$ indicated that the trends in the temporal change in P(ψ=1) were largely insignificant ($p > 0.1$) and not enough to reject H_0 for most groups. The exception is CV1, which was weakly significant (Table 2).

29

Crevasse Group	$\hat{\beta}_0$	$\hat{\beta}_1$	S.E.	$\hat{z}$	p-value ($\alpha=0.05$)	$e^{\hat{\beta}}$
CV1	1.5	-0.0002	0.00012	-1.7160	0.086	1
CV2	2.0316	0.0001	0.00017	0.6559	0.512	1
CV3	1.1213	0.0002	0.00014	1.6136	0.107	1
CV4	1.9422	-9.58E-7	0.00015	-0.0064	0.995	1
CV5	1.8507	-4.15E-5	0.00014	-0.3014	0.763	1
CV6	1.3976	-2.33E-5	0.00012	-0.1919	0.848	1
CV7	0.4823	9.03E-5	0.00011	0.8322	0.405	1

Table 2. Logit regression model parameters for all water-filled crevasse groups.

Chapter 5. Discussion

5.1 Impact of Sampling Bias

The impact of cloud cover and varying temporal resolution has a significant impact on how we interpret drain dynamics of the water-filled crevasses using our archive. These issues result in variation in the number of observations over the crevasse groups for each season. The numbers of samples used to characterize the hydrologic state of water-filled crevasses were fewer before 2009 than after. This raises the possibility that drainage events earlier in the study period were missed. Furthermore, the lack of daily sampling over all seasons means our estimates of drainage dates may not be exact. Drainage events were based on the observation of the lack of water present over a given CV group. Images were not necessarily obtained the same day a drainage occurred. However, in most cases, we were able to bound the time interval over which a particular CV group drained since most observations occurred on an interval of 10 days or less. Additional data from new sources, such as visible imagery from Cubesats, will be considered to improve sampling resolution for future studies.

5.2 Factors Influencing Drain Behavior

Everett et al. (2016) hypothesize that drainage and filling downstream of Helheim Glacier may be the result of a high pressure wave passing down glacier following a lake drainage. We have not observed coordination in drain and fill behaviors among adjacent pond groups. There is no relationship between supraglacial lake drainage and water-filled crevasse drainage within the shear margins of Jakobshavn as the closest lake to many of our CV groups is more than 15 km away in the extra-marginal ice field. Lastly, it is not feasible for drainage of crevasse groups within the northern margin to impact the filling and drainage behavior of those within the southern margin and vice versa. The margins are separated by a deep trough with no evidence for connected subglacial hydrology transverse to the main direction of ice flow.

For our study we considered that seasonal variability in surface temperatures responsible for melt production and runoff may be an important driver on the observed hydrologic state patterns. During seasons with relatively warmer temperatures, water-filled crevasses can demonstrate multiple drain and refill cycles. This process is facilitated by the capacity for short-term localized melt production and runoff, which could rapidly refill crevasses after a drainage event. However, in cooler seasons, there would be insufficient energy to drive rapid refilling after an initial drainage event. Surface temperatures have demonstrated a positive trend of 0.47±0.55 (°C/Decade) over central-west Greenland (Hall et al. 2013). Specifically, average near-surface temperatures near Jakobshavn over the study period varied between -1 to 2 °C. High frequencies of multi-drainage events corresponded to warmer seasons, while cooler periods had few to

any multi-drainage events. It is not clear that the occurrence of filled states over time is proportional to changes in regional temperature. This is also consistent in the logit model results as we might expect to see statistically significant trends in the probability of filled states with time commensurate with an increase in temperatures. The insignificance in the trend on the probability of filled states regardless of the sign seems to indicate that temperature is not a control on whether a given crevasse group will be more or less likely to be filled. It is likely that temperature is more influential in determining the seasonal areal extent of these water-filled crevasse groups. Since we did not assess the areal of extent of these system in this analysis, additional work is necessary to evaluate these relationships.

The water-filled crevasses examined in this analysis are in a field of closely-spaced fractures. An air-filled fracture in a field of other crevasses maintains a lower net stress intensity factor at the fracture tip, which requires a larger tensile stress to propagate the fracture to the bed (van der Veen 1998). Mean distance between fractures within the boundaries of the CV groups can range from ~78 m (CV7) to 110 m (CV3), which corresponds to stress intensity factors between ~0.5 to 0.7 (MPa $m^{1/2}$) (van der Veen 1998). These values exceed the ice fracture toughness (0.1 - 0.4 MPa $m^{1/2}$) (van der Veen 1998), but only for the case where the fractures are water-filled. A water-filled crevasse can readily penetrate to the bed because the density of water is greater than ice such that if the fracture remains water-filled, the resulting hydrostatic pressure is sufficient to overcome lithostatic pressures (van der Veen 1998, 2007). Therefore, the filling rate is the most important factor controlling fracture propagation (van der Veen 2007). Filling rates estimated during the 2007 melt season ranged from 0.04 to 1.25 (m h^{-1}) (Lampkin et

al. 2013). Given these rates, for a tensile stress of ~ 300 kPa, a single fracture could penetrate between ~400 to 1100 m, which is equivalent to ice thickness in the vicinity of the water-filled crevasses. Melt water production and runoff responsible for filling crevasses are variable both intra and inter-seasonally. This would induce intermittent hydrofracture crack propagation, and may not allow for a fracture to penetrate to the bed. Under these circumstances, delivery of meltwater to the bed could only be possible if local strain rates are sufficiently large to overcome the reduced stress intensity in the closely-spaced crevasse fields. Estimated strain rates during the 2007 season over the water-filled crevasse systems were sufficiently large (Lampkin et al. 2013).

In this analysis, maximum tensile strain rates have increased over the last 16 years and were correlated with an increase in multi-drain events. The events are likely driven by both an increase in melt production and local tensile stress. This is consistent with laser altimetry estimates of surface roughness, which show substantial variability within the shear margins relative to the main trough from 2003 to 2009 (Herzfeld et al. 2014). There was no expansion of roughness within the shear margins during this period of rapid thinning (10-15 m a^{-1}) (Herzfeld et al. 2014).

5.3 Terminus Perturbations and Crevasse Drainage

Ocean-induced terminal perturbations have been implicated in the observed acceleration and thinning in the lower trunk of the ice stream (Aschwanden et al. 2016; Holland et al. 2008; Joughin et al. 2008). Bondzio et al. (2015) assert that ice acceleration within the main trough of Jakobshavn increases strain along the shear margins, while amplifying rheological softening. Therefore, ice fracture toughness would be reduced enough to

33

easily facilitate fracture propagation. Bondzio et al. (2017) have established that the impact of calving would be limited to within 10 km of the terminus. Clearly, the impact of terminal perturbations on strain rates in the vicinity of the water-filled crevasse groups were negligible over much of the analysis period. It is only during recent seasons that the front has reached a position such that the lower elevation systems (CV1, 2, and 4) are within the 10-15 km range (Joughin et al. 2012) where longitudinal coupling from calving events could be influential. This may change as the terminus of Jakobshavn continues its rapid retreat.

Chapter 6. Conclusions

Controls on drainage and filling are a complex set of interacting factors that include surface melt production/runoff, and local/regional ice dynamics driving fracture propagation. Crevasse systems within Jakobshavn shear margins fill and drain annually, therefore the frequency in the occurrence of water alone is not sensitive to observed increases in temperature. However, pond extent and depth are likely to be sensitive to regional warming over the study period but was not examined in this work. Regardless of the limitations in our archive, each water-filled crevasse system experienced considerable variability in filling as a result of local variability of melt water production, accumulation, and storage capacity. The size and configuration of subglacial morphology is probably a first-order control on storage capacity and indirectly influences local strain rates, fracture propagation, and drainage. More work is required to assess factors that control the magnitude and rate of filling such as components in the surface energy balance (i.e. solar insolation and turbulent heat flux) or the potential for localized inter-fracture percolation.

The major findings in the study indicate that water-filled crevasse groups demonstrate differences in both spatial and temporal variability of hydrologic state that reflects local conditions in melt production, run-off, and drain behavior. Drainage frequency is not sensitive to increasing temperatures over the study period. Frequency of drainage increases with increasing strain rates though factors driving inter-seasonal changes in strain along the margins have not been evaluated. The impact of calving on drain behavior was negligible until the end of the study period, when the lower elevation crevasse systems were within ~10 km of the terminus. This may become an important factor in influencing water-filled crevasse systems in the future as the terminus continues to retreat. We discovered increased occurrence in multiple inter-seasonal drainage events, which may be related to dynamics of the subglacial hydrologic environment. Additional work is required to understand how englacial and subglacial systems impact drain propensity.

Enhanced mass flux from Jakobshavn Isbræ over the last couple of decades is driven by a combination of various factors. In particular, the impact of hydrologic weakening of the shear margins could increasingly become a major factor in both enhancing extra-marginal ice flow as well as amplifying the impact of ocean-induced terminal perturbations. Current trends and projections indicate a warmer arctic. Under prognostic scenarios, we could expect expansion in both the distribution of ponded water in the shear margins to higher elevations and areal extent. Large volumes of water would become available for infiltration driving regional changes in ice dynamics. Hydrologic weakening of the shear margins could play a critical role in the future stability of not only

Jakobshavn, but other outlet glaciers that have the presence of multimodal (lakes and water-filled/fractures/crevasses) supraglacial hydrologic systems.

References

Alley, R. B., P. U. Clark, P. Huybrechts, and I. Joughin, 2005a: Ice-Sheet and Sea-Level Changes. *Science*, **310**, 456–460, doi:10.1126/science.1114613. http://www.ncbi.nlm.nih.gov/pubmed/16239468.

Alley, R. B., T. K. Dupont, B. R. Parizek, and S. Anandakrishnan, 2005b: Access of surface meltwater to beds of sub-freezing glaciers: Preliminary insights. *Ann. Glaciol.*, **40**, 8–14, doi:10.3189/172756405781813483.

Aschwanden, A., M. A. Fahnestock, and M. Truffer, 2016: Complex Greenland outlet glacier flow captured. *Nat. Commun.*, **7**, 10524, doi:10.1038/ncomms10524.

Bartholomew, I., P. Nienow, D. Mair, A. Hubbard, M. A. King, and A. Sole, 2010: Seasonal evolution of subglacial drainage and acceleration in a Greenland outlet glacier. *Nat. Geosci.*, **3**, 408–411, doi:10.1038/ngeo863.

Benn, D. I., N. R. J. Hulton, and R. H. Mottram, 2007: "Calving laws", "sliding laws" and the stability of tidewater glaciers. *Annals of Glaciology*, Vol. 46 of, 123–130

Bondzio, J. H., H. Seroussi, M. Morlighem, T. Kleiner, M. Rückamp, A. Humbert, and E. Larour, 2015: Modelling the dynamic response of Jakobshavn Isbræ, West Greenland, to calving rate perturbations. *Cryosph. Discuss.*, **9**, 5485–5520, doi:10.5194/tcd-9-5485-2015.

Bondzio, J. H., and Coauthors, 2017: The mechanisms behind Jakobshavn Isbrae's acceleration and mass loss: A 3-D thermomechanical model study. *Geophys. Res. Lett.*, **44**, 6252–6260, doi:10.1002/2017GL073309.

Box, J. E., and K. Ski, 2007: Remote sounding of Greenland supraglacial melt lakes: Implications for subglacial hydraulics. *J. Glaciol.*, **53**, 257–265, doi:10.3189/172756507782202883.

Das, S. B., I. Joughin, M. D. Behn, I. M. Howat, M. A. King, D. Lizarralde, and M. P. Bhatia, 2008: Fracture Propagation to the Base of the Greenland Ice Sheet During Supraglacial Lake Drainage. *Science*, **320**, 778–781, doi:10.1126/science.1153360.

Echelmeyer, K., T. S. Clarke, and W. D. Harrison, 1991: Surficial glaciology of Jakobshavn Isbrae, West Greenland: Part I. Surface Morphology. *J. Glaciol.*, **37**, 368–382.

Everett, A., and Coauthors, 2016: Annual down-glacier drainage of lakes and water-filled crevasses at Helheim Glacier, southeast Greenland. *J. Geophys. Res. F Earth Surf.*, **121**, 1819–1833, doi:10.1002/2016JF003831.

Hall, D. K., J. C. Comiso, N. E. Digirolamo, C. A. Shuman, J. E. Box, and L. S. Koenig, 2013: Variability in the surface temperature and melt extent of the Greenland ice sheet from MODIS. *Geophys. Res. Lett.*, **40**, 2114–2120, doi:10.1002/grl.50240.

Hanna, E., and Coauthors, 2008: Increased runoff from melt from the Greenland Ice Sheet: A response to global warming. *J. Clim.*, **21**, 331–341, doi:10.1175/2007JCLI1964.1.

Herzfeld, U. C., and Coauthors, 2014: Elevation changes and dynamic provinces of Jakobshavn Isbræ, Greenland, derived using generalized spatial surface roughness from ICESat GLAS and ATM data. *J. Glaciol.*, **60**, 834–848, doi:10.3189/2014JoG13J129.

Hoffman, M. J., G. A. Catania, T. A. Neumann, L. C. Andrews, and J. A. Rumrill, 2011: Links between acceleration, melting, and supraglacial lake drainage of the western Greenland Ice Sheet. *J. Geophys. Res. Earth Surf.*, **116**, F04035, doi:10.1029/2010JF001934.

Holland, D. M., R. H. Thomas, B. de Young, M. H. Ribergaard, and B. Lyberth, 2008: Acceleration of Jakobshavn Isbræ triggered by warm subsurface ocean waters. *Nat. Geosci.*, **1**, 659–664, doi:10.1038/ngeo316.

Howat, I. M., S. de la Peña, J. H. van Angelen, J. T. M. Lenaerts, and M. R. van den Broeke, 2013: Brief Communication "Expansion of meltwater lakes on the Greenland Ice Sheet." *Cryosph.*, **7**, 201–204, doi:10.5194/tc-7-201-2013.

Howat, I. M., A. Negrete, B. E. Smith, 2015a: *MEaSUREs Greenland Ice Sheet Mapping Project (GIMP) Digital Elevation 30 Model*, Boulder, Colorado USA: NASA National Snow and Ice Data Center Distributed Active Archive Center. DOI: http://dx.doi.org/10.5067/NV34YUIXLP9W

Howat, I. M., A. Negrete, & B. Smith 2015b: The Greenland Ice Mapping Project (GIMP) land classification and surface elevation data sets. *The Cryosphere* 8: 1509-1518. doi: http://dx.doi.org/10.5194/tc-8-1509-2014

Joughin, I., S. Tulaczyk, M. Fahnestock, and R. Kwok, 1996: A Mini-Surge on the Ryder Glacier, Greenland, Observed by Satellite Radar Interferometry. *Science*, **274**, 228–230, doi:10.1126/science.274.5285.228.

Joughin, I., W. Abdalati, and M. Fahnestock, 2004: Large fluctuations in speed on

Greenland's Jakobshavn Isbræ glacier. *Nature*, **432**, 608–610,

doi:10.1038/nature03130.

Joughin, I., S. B. Das, M. A. King, B. E. Smith, I. M. Howat, and T. Moon, 2008:

Seasonal speedup along the western flank of the Greenland Ice Sheet. *Science*, **320**,

781–783, doi:10.1126/science.1153288.

Joughin, I., B. E. Smith, I. M. Howat, T. Scambos, and T. Moon, 2010: Greenland flow

variability from ice-sheet-wide velocity mapping. *J. Glaciol.*, **56**, 415–430,

doi:10.3189/002214310792447734.

Joughin, I., R. B. Alley, and D. M. Holland, 2012: Ice-sheet response to oceanic forcing.

Science, **338**, 1172–1176, doi:10.1126/science.1226481.

Joughin, I., Howat, I., Smith, B., & Scambos, T, 2016, MEaSUREs Greenland Ice

Velocity: Selected Glacier Site Velocity Maps from InSAR, Version 1. [Ice

Velocity]. Boulder, Colorado USA. NASA National Snow and Ice Data Center

Distributed Active Archive Center. doi:

http://dx.doi.org/10.5067/MEASURES/CRYOSPHERE/nsidc-0481.001.

Koenig, L. S., and Coauthors, 2015: Wintertime storage of water in buried supraglacial

lakes across the Greenland Ice Sheet. *Cryosphere*, **9**, 1333–1342, doi:10.5194/tc-9-

1333-2015.

Krabill, W., and Coauthors, 2004: Greenland Ice Sheet: Increased coastal thinning.

Geophys. Res. Lett., **31**, 1–4, doi:10.1029/2004GL021533.

Krawczynski, M. J., M. D. Behn, S. B. Das, and I. Joughin, 2009: Constraints on the lake

volume required for hydro-fracture through ice sheets. *Geophys. Res. Lett.*, **36**, L10501, doi:10.1029/2008GL036765.

Lampkin, D. J., 2011: Supraglacial lake spatial structure in western Greenland during the 2007 ablation season. *J. Geophys. Res. Earth Surf.*, **116**, F04001, doi:10.1029/2010JF001725.

Lampkin, D.J., and J. VanderBerg, 2011: A preliminary investigation of the influence of basal and surface topography on supraglacial lake distribution near Jakobshavn Isbrae, western Greenland. *Hydrol. Process.*, **25**, 3347–3355, doi:10.1002/hyp.8170.

Lampkin, D.J., N. Amador, B. R. Parizek, K. Farness, and K. Jezek, 2013: Drainage from water-filled crevasses along the margins of Jakobshavn Isbræ: A potential catalyst for catchment expansion. *J. Geophys. Res. Earth Surf.*, **118**, 795–813, doi:10.1002/jgrf.20039.

Luthcke, S. B., and Coauthors, 2006: Recent Greenland Ice Mass Loss by Drainage System from Satellite Gravity Observations. *Science*, **314**.

Mcmillan, M., P. Nienow, A. Shepherd, T. Benham, and A. Sole, 2007: Seasonal evolution of supra-glacial lakes on the Greenland Ice Sheet. *Earth Planet. Sci. Lett.*, 484–492, doi:10.1016/j.epsl.2007.08.002.

Nagler, T., Forsberg, R., Marcus, E., & Hauglund, K, 2017: Product User Guide (PUG) for the Greenland Ice Sheet CCI project of ESA's Climate Change Initiative, version 2.1, http://www.esa-icesheets-greenland-cci.org/

Nye, J. F., 1955: Comments on Dr. Loewe's Letter and Notes on Crevasses. *J. Glaciol.*,

2, 512–514, doi:10.1017/S0022143000032652.

Nye, J. F., 1957: The distribution of stress and velocity in glaciers and ice sheets. *Proc. Roy. Soc. Lond.*, **239**, 113–133.

Palmer, S., A. Shepherd, P. Nienow, and I. Joughin, 2011: Seasonal speedup of the Greenland Ice Sheet linked to routing of surface water. *Earth Planet. Sci. Lett.*, **302**, 423–428, doi:10.1016/j.epsl.2010.12.037.

Rignot, E., J. E. Box, E. Burgess, and E. Hanna, 2008: Mass balance of the Greenland ice sheet from 1958 to 2007. *Geophys. Res. Lett.*, **35**, L20502, doi:10.1029/2008GL035417.

Selmes, N., T. Murray, and T. D. James, 2011: Fast draining lakes on the Greenland Ice Sheet. *Geophys. Res. Lett.*, **38**, n/a-n/a, doi:10.1029/2011GL047872.

Shepherd, A., A. Hubbard, P. Nienow, M. King, M. McMillan, and I. Joughin, 2009: Greenland ice sheet motion coupled with daily melting in late summer. *Geophys. Res. Lett.*, **36**, L01501, doi:10.1029/2008GL035758.

Shepherd, A., and Coauthors, 2012: A Reconciled Estimate of Ice-Sheet Mass Balance. *Science (80-.).*, **338**, 1183–1189, doi:10.1126/science.1228102..

Sneed, W. A., and G. S. Hamilton, 2007: Evolution of melt pond volume on the surface of the Greenland Ice Sheet. *Geophys. Res. Lett.*, **34**, L03501, doi:10.1029/2006GL028697.

Steffen, K., J. E. Box, W. Abdalati, 1996: Greenland Climate Network: GC-Net, Colbeck, S. C. Ed. CRREL 96-27 Special Report on Glaciers, Ice Sheets and Volcanoes, trib. to M. Meier, 98-103.

Sundal, A. V., A. Shepherd, P. Nienow, E. Hanna, S. Palmer, and P. Huybrechts, 2009: Evolution of supra-glacial lakes across the Greenland Ice Sheet. *Remote Sens. Environ.*, **113**, 2164–2171, doi:10.1016/j.rse.2009.05.018.

Sundal, A. V., A. Shepherd, P. Nienow, E. Hanna, S. Palmer, and P. Huybrechts, 2011: Melt-induced speed-up of Greenland ice sheet offset by efficient subglacial drainage. *Nature*, **469**, 521–524, doi:10.1038/nature09740.

Tedesco, M., and N. Steiner, 2011: In-situ multispectral and bathymetric measurements over a supraglacial lake in western Greenland using a remotely controlled watercraft. *Cryosphere*, **5**, 445–452, doi:10.5194/tc-5-445-2011.

van den Broeke, M., and Coauthors, 2009: Partitioning recent Greenland mass loss. *Science*, **326**, 984–986, doi:10.1126/science.1178176.

Van der Veen, C. J., 1998: Fracture mechanics approach to penetration of surface crevasses on glaciers. *Cold Reg. Sci. Technol.*, **27**, 31–47, doi:10.1016/S0165-232X(97)00022-0.

Van der Veen, C. J., 1999: Crevasses on glaciers. *Polar Geogr.*, **23**, 213–245, doi:10.1080/10889379909377677.

Van der Veen, C. J., 2007: Fracture propagation as means of rapidly transferring surface meltwater to the base of glaciers. *Geophys. Res. Lett.*, **34**, L01501, doi:10.1029/2006GL028385.

van de Wal, R. S. W., W. Boot, M. R. van den Broeke, C. J. P. P. Smeets, C. H. Reijmer, J. J. A. Donker, and J. Oerlemans, 2008: Large and rapid melt-induced velocity changes in the ablation zone of the Greenland Ice Sheet. *Science*, **321**, 111–113, doi:10.1126/science.1158540.

Zwally, H. J., W. Abdalati, T. Herring, K. Larson, J. Saba, and K. Steffen, 2002: Surface Melt-Induced Acceleration of Greenland Ice-Sheet Flow. *Science*, **297**.